Correlation of Temperature Dependence of Gas Permeability with Pore Size in Molecular Sieving Membranes: A Grand Canonical Ensemble Molecular Dynamics Study

Hiromitsu Takaba,* Eriya Matsuda, and Shin-ichi Nakao

Department of Chemical System Engineering, The University of Tokyo, 7-3-1 Hongo Bunkyo-ku, Tokyo 113-8685, Japan

Received: March 2, 2004; In Final Form: June 18, 2004

The transition boundary of the temperature dependence of small gas permeability through molecular sieving membranes was investigated by the use of grand canonical ensemble molecular dynamics (GCMD). The temperature dependence of H_2, Ne, Ar, O_2, N_2, and CO_2 permeability through molecular sieving membranes was examined by use of membrane models having cylindrical pores with a range of 0.3−0.5 nm. Our simulation successfully demonstrated that the observed permeability varied from nonactivated transport to activated transport with increasing temperature as the pore size of the membrane models approached the molecular diameter of the permeating species. This suggests that the permeation mechanism changed to molecular sieving. Activated transport was found when the pore size of the membrane became smaller than 1.2 times that of the molecular diameter of the permeating species. There was no clear correlation observed between the static interaction between the gas and pore wall and the transition boundary of the temperature dependence of permeability. The observed activation energy for permeation was in the range of 1−7 kJ/mol, dependent on the permeating species.

1. Introduction

Molecular sieving membranes have been attractive options for various separation processes because of their high separation capability based on their microporous structure. Silica membranes in particular, with pores smaller than 0.5 nm, are capable of showing molecular sieving for small inorganic and hydrocarbon gases.[1−6] The observed gas permeability of these membranes was activated with increasing temperature, and the activation energies for the small gases were in the range 6−22 kJ/mol.[2,3] Conversely, the permeability of silica membranes having larger pore sizes (>1 nm) was not activated with increasing temperature and no longer showed molecular sieving. However, the transition conditions of the temperature dependence of permeability from nonactivated transport to molecular sieving are still obscure, because of the lack of a direct measurement method to quantify the accurate pore sizes of molecular sieving membranes. Better understanding of activated transport in molecular sieving membranes is required to develop more efficient molecular sieving membranes.

In general, activated transport in microporous materials is considered a result of interactions of the permeating species with the pore wall. As the pore size narrows, the attractive interaction of the permeating species with atoms in the circumference of the pore wall shows a maximum at a certain pore size, whereas further narrowing of the pore gives a repulsive interaction. This idea has been used to explain the drastic change in activation energy of the permeability observed in experiments. Shelekhin et al.[7] proposed a mathematical model of gas permeation in microporous molecular sieving membranes. According to their model, permeability is a function of both a kinetic part and an activated part, and this corresponds to a permeation mechanism based on a transition from Knudsen diffusion to activated transport. Xiao and Wei[8] proposed a theoretical model for single-component diffusion of hydrocarbons in zeolites, based on molecule−zeolite and molecule−molecule interactions. Transition from the Knudsen regime to the activated transport regime in ZSM-5 was predicted for spherical molecules with a ratio of molecular diameter to channel diameter in the range of 1.25−1.67. However, their models were based on a static energy calculation inside the pore, and the resistance at the surface, or pore mouth, was not considered.

Molecular simulation techniques are also considered powerful tools to investigate the correlation of permeation mechanisms with pore size. Ahunbay et al.[9] investigated the diffusion mechanism of methane in a silicalite single-crystal membrane by the dual control volume grand canonical ensemble molecular dynamics method and concluded that surface resistance could significantly affect gas permeability when a molecule larger than methane permeates through a polycrystalline membrane. Some groups have supported this idea, termed "interface resistance". Skoulidas and Sholl[10] performed equilibrium molecular dynamics simulations to examine the kinetic selectivity of molecular species such as ethane, *n*-butane, and *n*-hexane when they enter the circular mouth of a micropore. According to their investigation, the number of molecules that could enter the pore mouth became smaller with the increase in the carbon number of the molecule, and they concluded that transport through microporous crystals was influenced by steric selectivity at the pore mouth. We have carried out nonequilibrium molecular dynamics (MD) to investigate the permeation mechanism of inorganic gases (CO_2, N_2, He, etc.) occurring in silica membranes with pore sizes less than 0.5−1.0 nm[11,12] and included the surface effect in these calculations. The permeability of the investigated gases did not show any activated transport with increasing temperature. Yoshioka et al.[13] also performed nonequilibrium MD for investigations of CO_2 and N_2 permeation through a cylindrical pore (pore size was 0.8 nm), and nonactivated temperature

* Corresponding author: Tel and fax +81-3-5841-7300; e-mail takaba@chemsys.t.u-tokyo.ac.jp.

10.1021/jp049068h CCC: $27.50
Published on Web 08/21/2004

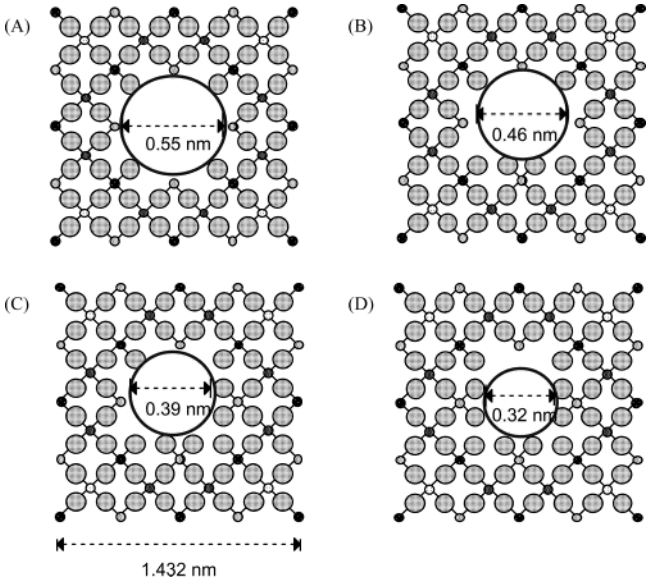

Figure 1. Surface view of four membrane models with different pore sizes. The pore sizes of individual models of A, B, C, and D are 0.55, 0.46, 0.39, and 0.32 nm, respectively.

dependence of permeability was reported. The pore sizes in these studies were too large to observe activated transport. Nonequilibrium MD of amorphous silica membranes has been also reported by Pohl and Heffelfinger.[14] Their membranes modeled an amorphous glass with a pore size distribution that was less than 0.34 nm. The temperature dependence of He and N_2 permeation was found to be nonactivated, in contrast to experimental observations.[3,5] To our knowledge, activated transport of lightweight gases in inorganic membranes has not been reported by use of molecular simulations, although this is the most familiar observation in experiment.

In this study, we applied the grand canonical ensemble molecular dynamics method (GCMD) to the transport of inorganic gases through model membranes having cylindrical pores. The objective of this study was to investigate the relationship between pore size and temperature dependence of permeability and to clarify the pore size in which molecular sieving is expected.

2. Calculation

2.1. Membrane Models. The membrane models were created by removing SiO atom pairs from a β-cristobalite containing 216 Si and 432 O atoms with dimensions 2.148 × 2.148 × 2.148 nm. Figure 1 presents the surface view of four membrane models (models A−D). The pore sizes of these models are 0.55, 0.46, 0.39, and 0.32 nm, respectively. The pore size was calculated on the basis of the atomic radius of oxygen, 0.17 nm, which was the size parameter in Lennard-Jones potential. The pore size of silica membranes capable of showing molecular sieving is less than about 0.5 nm, so some of our membrane models were expected to show molecular sieving. Because the dimension of the pore is in the range of an atomic radius, the pore structure is not smooth and round but is rather rough at the atomic scale. Figure 2 illustrates the detailed structure of the pore wall and pore mouth of model D. As shown in this figure, the pore mouth is almost a rectangle, and the pore wall is rugged and forms atomic cages.

Although actual silica surface is regularly terminated by OH groups, we modeled the bare silica surface. Since the interaction between polarized OH group and investigated gases is considered to be very weak, the influence from OH group on permeation behavior will be negligible.

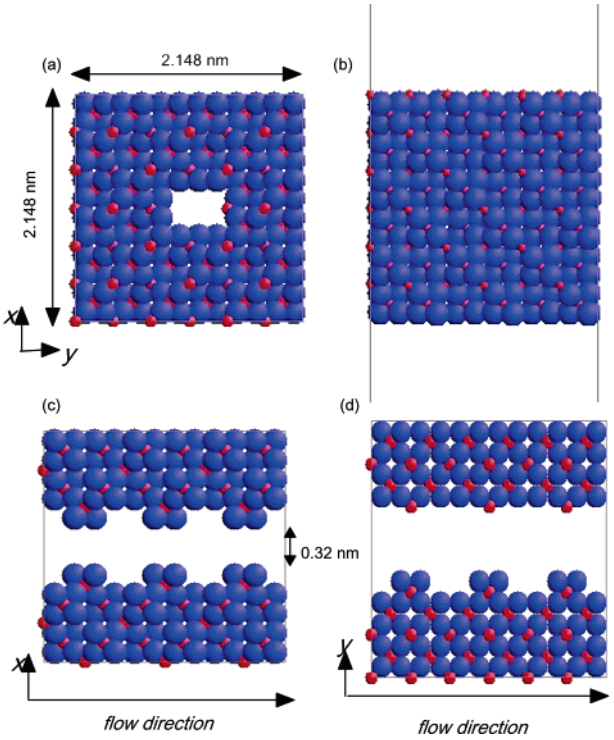

Figure 2. Pictures of the surface and cross-sectional views of the pore in model D. The bigger atoms represent oxygen atoms and smaller ones represent silicon atoms. (a) Surface view; (b) side view; (c, d) cross-sectional views.

The membranes we modeled were rather thin in comparing experimental membranes. Molecular simulations applied to very thin membranes are often dominated by surface effects that may be considerably less important for membranes of practical experimental thickness. Some literature pointed out surface effect and suggested a complementary modeling method in zeolite membranes.[15−17] However, silica molecular sieving membranes have inhomogeneous structure. Thus, the thickness of membrane model for reproducing activated transport will be thinner than the reported membrane thickness. Our model may be adequate as a first attempt to investigate activated transport in molecular sieving membranes.

2.2. Grand Canonical Ensemble Molecular Dynamics. The GCMD method has been used to investigate pressure-driven gas transport through porous inorganic membranes.[11,18−20] GCMD combines molecular dynamics (MD) with grand canonical Monte Carlo (GCMC) methods to reproduce the pressure drop across the membrane. The GCMD unit cell is divided into four regions: the buffer region, I; the gas region, II; the membrane region, III; and the vacuum region, IV. The chemical potentials of the gas and vacuum regions are maintained at particular values by the GCMC method. A GCMC calculation incorporating the insertion and deletion of diffusing particles is performed, followed by a series of MD calculations for all particles existing throughout all four regions. The pressure drop between the gas and vacuum regions is introduced by setting the chemical potential high in the gas region and low in the vacuum region. Consequently, steady-state diffusion from the gas region to the vacuum region occurs through the membrane region. We set a buffer region I between the gas and the vacuum regions to avoid the rapid change of molecular density between gas and vacuum regions. Molecules can diffuse to region I from

TABLE 1: Activities Used in the GCMD Simulations[a]

	activity ($1/A^3$)	
temp (K)	region I	region IV
300	0.0050	0.0001
400	0.003 75	0.0001
410	0.003 66	0.0001
450	0.0033	0.0001
500	0.0030	0.0001
600	0.0025	0.0001

[a] Activities were designed to keep the feed pressure at almost the same value for all simulations irrespective of temperature. The same activities were applied for all gas species.

region II, and those diffusing into region IV are removed immediately.

The particle insertion and deletion algorithms in the sequence of GCMD were carried out on the basis of Adams's GCMC algorithm.[21,22] A velocity conforming to the mean velocity of the Maxwell−Boltzmann distribution at the specified temperature was assigned to each newly created molecule. Streaming velocity[9] was not added to the newly created molecule. Because the porosity of our modeled membrane was rather small, especially in model D, almost molecules diffused in the gas region and were deleted before permeating through the membrane by GCMC procedure. Hence, the addition of the streaming velocity would cause inadequate velocity distribution in our system. The equations of motion were numerically integrated by the Verlet leapfrog algorithm with a 2.0 fs time step to produce a trajectory of atoms under the three-dimensional periodic boundary condition. The temperature of the diffusing molecules was controlled at a specified temperature for each separate region by means of a scaling method.[12] Because of small number of molecules in each region, the instantaneous calculated temperatures in each region were sometimes inhomogeneous. However, the average temperatures during the simulation in each region were nearly at a specified temperature. In the following calculations, the temperature means that of the average of whole diffusing molecules. As one GCMD step, 50 MD steps were carried out after 100 GCMC steps for each gas and the vacuum region. The total simulation time was 500 000−1 500 000 MD steps, corresponding to 1−3 ns in real time. The pressure of feed gas was estimated from an average density of atoms in region II, assuming the ideal gas equation.

The dimension of the unit cell used for GCMD simulations was 1.9635 × 2.0793 × 10.0000 nm, including one pore, and the membrane area was 4.0828 nm^2. The sizes of each cell (I, II, III, and IV) along the *z* direction were 0−1.0 nm, 1.0−3.0 nm, 3.0−7.5 nm, and 7.5−10.0 nm, respectively.

The activities used in the following GCMD simulations are summarized in Table 1, which gives pressures in regions II and IV in the range of 50−70 and 0 atm, respectively. In this region, the adsorption of gas in the model membrane is nearly in the Henry region; thus the permeability is expected to be proportional to the applied pressure. Permeability is calculated as

$$P = \frac{Nd}{A\Delta t \Delta p N_A} \tag{1}$$

where N is the number of molecules permeating to the vacuum region IV, d is the membrane thickness, A is the membrane area, Δt is the simulation time, ΔP is the pressure difference across the membrane, and N_A is Avogadro's number.

The 12-6 Lennard-Jones (LJ) type potential was used to represent a nonbonded interaction between diffusing particles and atoms in a membrane, shown below as

TABLE 2: Potential Parameters Used in the 12-6 L-J Function

	σ_{ii} (× 10^{-1} nm)	ϵ_{ii}/k_B[a] (K)	ref
Ne	2.820	32.80	23
H_2	2.827	59.70	23
O_2	3.467	106.70	23
Ar	3.542	93.30	23
N_2	3.798	71.40	23
CO_2	3.941	195.20	23
Si (silica)	0.000	0.0	24
O (silica)	3.000	230.00	24

[a] k_B is the Boltzmann constant.

$$E = \sum 4\epsilon[(\sigma/r_{ij})^{12} - (\sigma/r_{ij})^{6}] \tag{2}$$

Lorentz−Berthelot theory[23] was applied for the heteroatomic interaction. In GCMD simulations, the atoms in the membrane were treated as rigid and the interaction of a gas atom with a Si atom was neglected to reduce the computational cost. The cutoff length was 0.851 25 nm. The potential parameters used are summarized in Table 2.

The permeability obtained from GCMD was analyzed on the basis of a permeation model. Two theoretical models have been proposed as permeation models for molecular sieving membranes. According to Xiao and Wei,[8] the permeability through a molecular sieving membrane can be described as

$$P = \alpha \exp\left(\frac{-\Delta E}{RT}\right) \tag{3}$$

where ΔE is the activation energy for permeation, α is a constant, R is the gas constant, and T is the temperature. Shelekhin et al.[7] also described a theory for activated transport in a molecular sieving glass, which has large pores inside the membrane that interconnect each other through narrower pores. They described the permeability in those membranes as

$$P = \frac{\beta}{\sqrt{MT}} \exp\left(\frac{-\Delta E}{RT}\right) \tag{4}$$

where M is the molecular weight of the permeating molecule and β is a constant related to the pore structure. Because the dependency of temperature in the second term is so large compared with that in the first term, the temperature dependence of permeability calculated from eqs 3 and 4 shows no significant difference. In this paper, therefore, we used eq 3 as a description of temperature dependence of permeability.

3. Results and Discussion

The density profile of N_2 permeating in the unit cell along the flow direction for model C at 300 K is shown in Figure 3. The density of region II was found to be uniform, and the density in region III gradually increased approaching the membrane surface. The density in region IV was almost zero, meaning that the vacuum condition was achieved there. The density in the position where the membrane is located (region IV) was almost uniform and kept almost constant from the inlet to the outlet of the membrane. Condensation of N_2 in the pore was not observed. Similar density profiles were observed for all simulations.

Calculated permeabilities are shown as an inverse function of temperature in Figures 4−9. As shown in these figures, the magnitude of permeability for all permeating species decreased

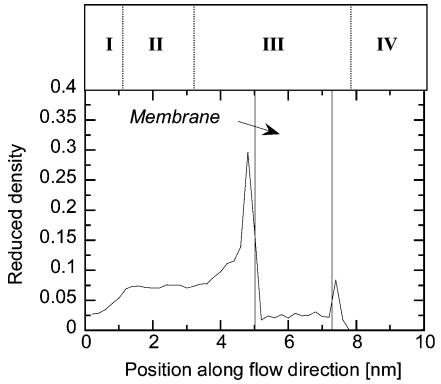

Figure 3. Density profile of N_2 in the unit cell along the flow direction in model C at 300 K. Reduced densities were calculated from the number of molecules divided by $\rho\sigma_{N_2}^3$, where ρ is the molecular density at that region.

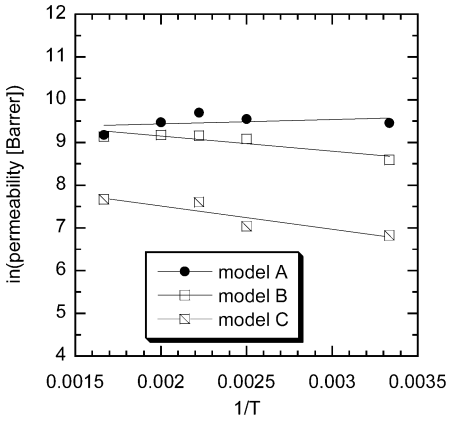

Figure 4. Calculated permeability for CO_2 in three different models as an inverse function of temperature.

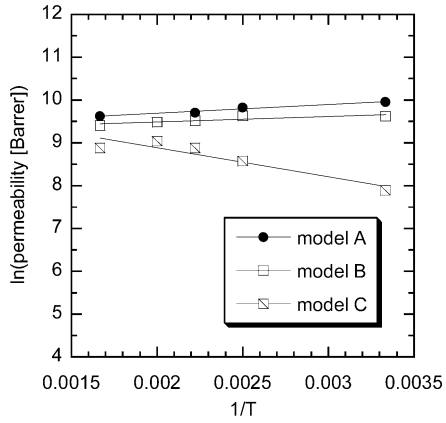

Figure 5. Calculated permeability for N_2 in three different models as an inverse function of temperature.

as the membrane pore size became smaller. In the case of CO_2 (Figure 4), the permeability in models B and C increased with increasing temperature, whereas the permeability in model A decreased with increasing temperature. CO_2 did not penetrate in model D. Consequently, activated transport of CO_2 with increasing temperature was observed when the ratio of the pore diameter and the molecular diameter of CO_2 was less than 1.16.

For N_2 (Figure 5), the differences in permeability between the models were small over the investigated temperature range, and the increase in permeability with increasing temperature was observed only for model C. N_2 did not permeate through model D during the simulated time. The difference in permeability between models for N_2 is smaller than that for CO_2. This

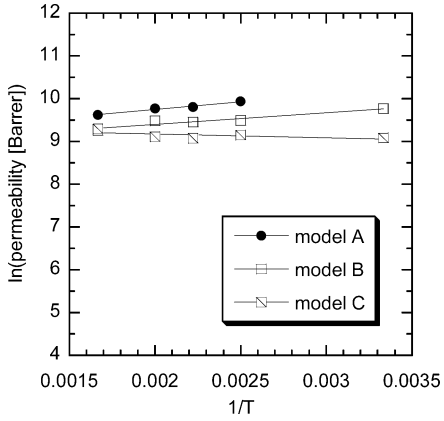

Figure 6. Calculated permeability for Ar in three different models as an inverse function of temperature.

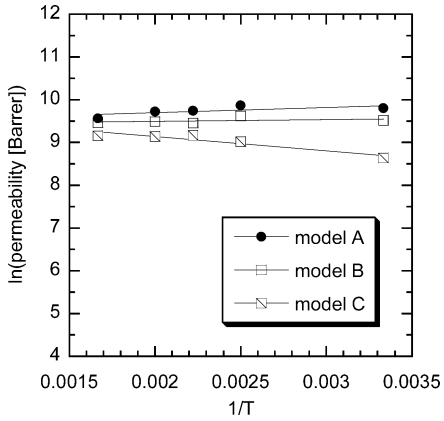

Figure 7. Calculated permeability for O_2 in three different models as an inverse function of temperature.

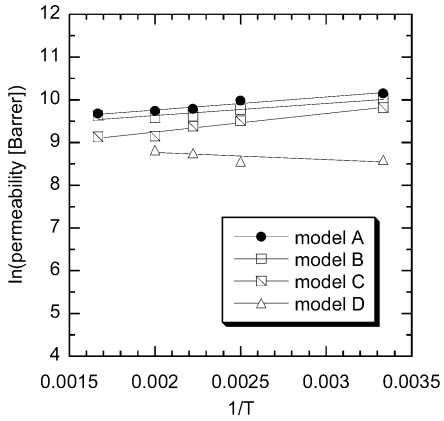

Figure 8. Calculated permeability for Ne in four different models as an inverse function of temperature.

will be because of their molecular size. As the molecular size becomes larger, the steric hindrance at pore mouth becomes larger. The pore size of model D is very close to the molecular size of CO_2, which results in the drastic decrease of permeability for CO_2 in model D. The ratio of the pore diameter of model C and the molecular diameter of N_2 was 1.02. The temperature dependences of Ar and O_2 permeability (Figures 6 and 7) were similar to that of N_2; activated transport was only observed for model C. The ratios of the pore diameter to the molecular diameter of Ar and O_2 in model C were 1.09 and 1.11, respectively.

Ne and H_2 permeated through all models (Figures 8 and 9). The temperature dependencies of their permeability were very similar; nonactivated transport was observed in models A−C,

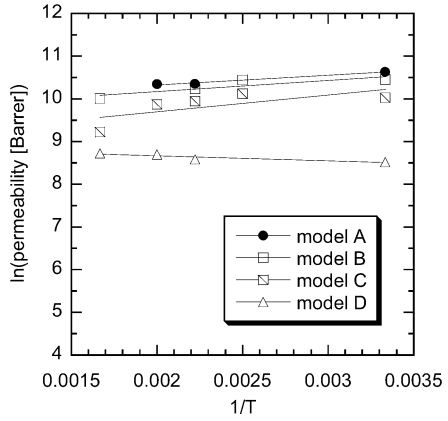

Figure 9. Calculated permeability for H_2 in four different models as an inverse function of temperature.

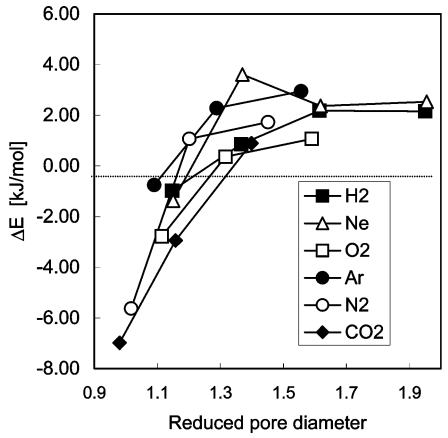

Figure 10. Correlation of the deduced pore diameter (pore diameter/σ_{ii}) and the activation energy for permeation.

and activated transport was observed in model D. The ratios of pore diameter and molecular diameter of Ne and H_2 in model D are 1.15.

Although activated transport with increasing temperature was observed for all gases, the observed temperature dependence differed slightly between gases. The slope of the plot for CO_2 gradually changed from positive to negative; however, the changes for other gases were more drastic. This may be because the relatively strong interaction of CO_2 with the pore wall contributed to activated transport. It is noted that activated transport was observed for all permeating species when the ratio of pore diameter to molecular diameter was less than 1.2. As no permeation occurred when the ratio is less than 1.0, the range of pore diameters in which activated transport is expected is very narrow; for example, for N_2 this range is only 0.114 nm. Figure 10 represents the correlation of the deduced pore diameter (a ratio of pore diameter and molecular diameter σ_{ii}) with the activation energy (ΔE) for permeation calculated from eq 3. This figure clearly shows that permeation through the membranes changed from nonactivated transport to activated transport in the ratio range of 1.1−1.3. This range seems to be independent of gas species in this study. The magnitude of the activation energies for the investigated gases was in the range of 1−7 kJ/mol. These values are much smaller than experimentally determined values.[2,3] This implies that another factor, in addition to pore size, contributes to the determination of an experimental activation energy for permeation through silica membranes. Thermal vibration of pore framework, which equilibrium pore size is nearly equal to molecular size, might influence the determination of activation energy.

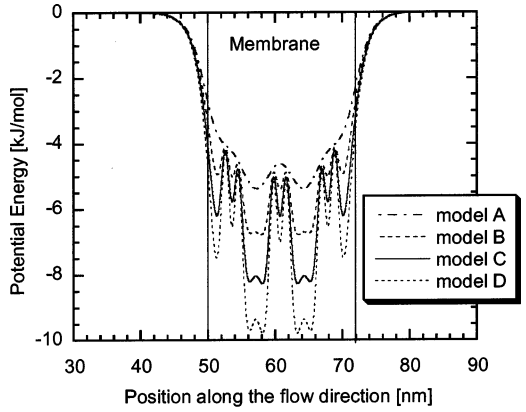

Figure 11. Profile of the static interaction energy between one H_2 molecule and atoms in the pore when an H_2 molecule goes through the center of the pore.

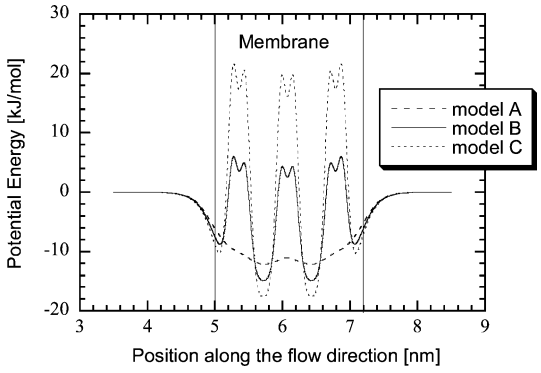

Figure 12. Profile of the static interaction energy between one Ar atom and atoms in the pore when an Ar atom goes through the center of the pore.

TABLE 3: Estimated Static Interaction Energy between the Gas Molecule and Atoms in Pore Walls[a]

	pore model			
	A	B	C	D
H_2	−1.70	−2.21	−2.91	−3.64
Ne	−5.38	−6.78	−8.28	−9.80
O_2	−3.96	−5.00	−6.11	−7.23
Ar	−12.30	−15.10	−17.90	
N_2	−12.20	−14.90	−17.60	
CO_2	−12.60	−15.30	−17.90	

[a] The highest energy obtained during diffusion through the center of the pore is indicated. Energies are given in kilojoules per mole.

Activated transport with increasing temperature implies the presence of an energetic barrier in the permeation path. Figures 11 and 12 represent the interaction energy profile of H_2 and Ar with atoms making up the pore wall. These are profiles of a static interaction energy where one molecule interacts with the pore wall during the diffusion along the line on the center of the pore. The profiles of Ne and O_2 were similar to that of H_2, and the profiles of N_2 and CO_2 were similar to that of Ar (they are not presented). As shown in these figures, plural transport barriers are found in the membrane region. By comparison with the temperature dependence of permeability shown in Figures 4−9, activated transport was not always observed even if the transport barrier existed in the permeation path. Table 3 summarizes the interaction energy of gases with atoms in the pore wall for all models; the highest energy barriers were chosen and indicated. The interaction energy of CO_2 with the pore wall in model A was much larger than that of H_2 in model D; however, activated transport of CO_2 was not observed in model

A, although activated transport of H_2 was observed in model D. This means that there is no clear correlation of static interaction between gas and pore wall with the transition boundary of temperature dependence of permeability. This also implies that the repulsive interaction between the pore wall and the permeating species predominantly determines the temperature dependence of permeability.

Conclusion

The transition boundary between activated and nonactivated transport with increasing temperature for gas molecule permeation through molecular sieving membranes was investigated by the use of GCMD. A model having pore diameters in the range between 0.3 and 0.6 nm was used as a membrane model of molecular sieving membranes, and H_2, Ne, Ar, O_2, N_2, and CO_2 were considered as the permeating gas species. Our simulation demonstrated that the temperature dependence of permeability varied from nonactivated transport to activated transport when the ratio of the pore diameter to the molecular diameter of the permeating gas was between 1.1 and 1.3. The calculated activation energies for permeation were in the range of 1−7 kJ/mol, depending on the permeating species. There was no clear correlation between the temperature dependence of permeability and the static interaction between a gas molecule and the pore wall. In this study our used models have the cage pore structures. Static interaction analysis results implied that the interaction originated from the cage's structure was not the main factor to determine the transition regime of activated transport. The steric hindrance at the pore mouth will be an important factor to determine temperature dependence of permeability.

The observed activation energies for permeation were smaller than experimental values observed for the same gas permeation through silica molecular sieving membranes. The activation energy of permeation may be sensitive to the potential parameter used; however, since the interactions of molecular sieving silica with the investigated inorganic gases are considered very weak, small differences in potential parameters are not expected to change permeation behavior drastically. In such a system, a repulsive region in potential will be more important in determination of temperature dependence of permeability. Hence, this result suggests that factors in addition to pore size, for example, thermal vibration of the silica framework, affect the temperature dependence of permeability in silica molecular sieving membranes.

References and Notes

(1) Kitao, S.; Asaeda, M. *J. Chem. Eng. Jpn.* **1990**, *23*, 367−370.
(2) Nair, B. N.; Keizer, K.; Okubo, T.; Nakao, S. I. *Adv. Mater.* **1998**, *10*, 249−250.
(3) de Lange, R. S. A.; Keizer, K.; Burggraaf, A. J. *J. Membr. Sci.* **1995**, *104*, 81−100.
(4) Brinker, C. J.; Hurd, A. J.; Schunk, P. R.; Frye, G. C.; Ashley, C. S. *J. Non-Cryst. Solids* **1992**, *147*, 424−436.
(5) Gavalas, G. R.; Megiris, C. E.; Nam, S. W. *Chem. Eng. Sci.* **1989**, *44*, 1829−1835.
(6) Tsapatsis, M.; Gavalas, G. *J. Membr. Sci.* **1994**, *87*, 281−296.
(7) Shelekhin, A. B.; Dixon, A. G.; Ma, Y. H. *AIChE J.* **1995**, *41*, 58−67.
(8) Xiao, J.; Wei, J. *Chem. Eng. Sci.* **1992**, *47*, 1123−1141.
(9) Ahunbay, M. G.; Elliott, J. R.; Talu, O. *J. Phys. Chem. B* **2002**, *106*, 5163−5168.
(10) Skoulidas, A. I.; Sholl, D. S. *J. Chem. Phys.* **2000**, *113*, 4379−4387.
(11) Takaba, H.; Matsuda, E.; Nair, B. N.; Nakao, S. *J. Chem. Eng. Jpn.* **2002**, *35*, 1312−1321.
(12) Takaba, H.; Mizukami, K.; Kubo, M.; Fahmi, A.; Miyamoto, A. *AIChE J.* **1998**, *44*, 1335−1343.
(13) Yoshioka, T.; Tsuru, T.; Asaeda, M. *Sep. Purif. Technol.* **2001**, *25*, 441−449.
(14) Pohl, P. I.; Heffelfinger, G. S. *J. Membr. Sci.* **1999**, *155*, 1−7.
(15) Skoulidas, A. I.; Bowen, T. C.; Doelling, C. M.: Falconer, J. L.; Noble, R. D.; Sholl, D. S. *J. Membr. Sci.* **2003**, *227*, 123−136.
(16) Bowen, T. C.; Falconer, J. L.; Noble, R. D.; Skoulidas, A. I.; Sholl, D. S. *Ind. Eng. Chem. Res.* **2002**, *41*, 1641−1650.
(17) Nagumo, R.; Takaba, H.; Nakao, S. *J. Phys. Chem. B* **2003**, *107*, 14422−14428.
(18) Heffelfinger, G. S.; Vanswol, F. *J. Chem. Phys.* **1994**, *100*, 7548−7552.
(19) Cracknell, R. F.; Nicholson, D.; Quirke, N. *Phys. Rev. Lett.* **1995**, *74*, 2463−2466.
(20) MacElroy, J. M. D. *J. Chem. Phys.* **1994**, *101*, 5274−5280.
(21) Adams, D. J. *Mol. Phys.* **1974**, *28*, 1241−1252.
(22) Adams, D. J. *Mol. Phys.* **1975**, *29*, 307−311.
(23) Reid, R C.; Prausnitz, J. M.; Sherwood, T. K. In *The Properties of Gases and Liquids*; McGraw-Hill: New York, 1988.
(24) MacElroy, J. M. D.; Raghavan, K. *J. Chem. Phys.* **1990**, *93*, 2068−2079.